RSC Applied Polymers

ROYAL SOCIETY OF CHEMISTRY

PAPER

View Article Online
View Journal

Cite this: DOI: 10.1039/d6lp00120c

Tailoring fully biobased optical adhesives *via* hydrogen-bonding modulation

Benjamin R. Nelson, [a,b] Vincent Scholiers, [a,c] Audrey H. Sakamoto,[a] John F. Rynk,[d] Paula A. Pranda,[a] Filip E. Du Prez, [c] Kristi S. Anseth [a,b,d] and Christopher N. Bowman *[a,d]

Received 6th April 2026,
Accepted 1st June 2026

DOI: 10.1039/d6lp00120c

rsc.li/rscapplpolym

Display technologies require optical adhesives that simultaneously provide high optical clarity, refractive index control, low birefringence and adhesive strength. However, many commercial adhesive systems rely on petroleum-derived acrylates and isocyanate-based urethanes. Herein, a fully biobased optical adhesive is reported that exploits the initiator-free photopolymerization of dithiolanes. Furthermore, hydrogen bond strength is modulated within the prepared adhesives by changing the chemistry with which the dithiolane is conjugated to a macromolecular core, allowing manipulation of properties including glass transition temperature, adhesion, refractive index, and other optical properties. Throughout these variations, all materials maintain high optical performance, exhibiting visible light transmittance above 98% and haze below 0.7%, coupled with low optical dispersion. These results demonstrate that dithiolanes are readily applied as initiator-free crosslinkers for the formulation of fully biobased optical adhesives.

Introduction

Optical adhesives are crucial components of modern display technologies, where multilayer stacks of functional films are laminated to control the propagation of light through focusing, polarization, brightness enhancement, and diffusion. Interfaces between layers must provide high optical clarity, precise refractive index matching, low birefringence, low dispersion, and robust stability over time. As display architecture becomes both thinner and more flexible, these demands intensify, requiring materials that combine mechanical robustness with finely tuned optical properties, and reduced yellowing over time.[1] Most commonly, optical adhesives rely on a UV-curable (meth)acrylate, often incorporating urethane linkages to improve hydrogen bonding, to transform from a spreadable and wettable liquid during application into a robust solid, interfacial coating after polymerization.[2,3] However, utilizing both acrylates and urethanes derived from isocyanates inherently ties optical adhesives to petroleum sources.

The desire to move away from petroleum-based sources has accelerated interest in biobased polymers for high-performance applications.[4–7] Among renewable carbon sources, dimers derived from fatty acids are increasingly used, especially in the production of adhesives.[8–12] Commercially available dimer derivatives, such as Priamine and Pripol, provide long hydrophobic aliphatic backbones with low viscosities and glass transition temperatures, allowing for inherent flexibility. When coupled with photopolymerizable moieties, these cores are advantageous building blocks for the creation of optical adhesive formulations.[13]

1,2-Dithiolanes are an intriguing class of cyclic five-membered disulfide-containing rings that have recently attracted renewed attention and are often derived from naturally occurring resources. Moreover, these functional groups combine several features that make them attractive building blocks for the development of biobased optical materials. For instance, the inherent ring strain of the cyclic disulfide renders them more reactive than their linear counterparts.[14] Since their absorption spectra is red shifted into the visible region, 1,2-dithiolanes undergo photopolymerization without the need for exogenous (and often colored) photoinitiators.[15,16] Furthermore, the ring-opening polymerization of 1,2-dithiolanes yields dynamically active (linear) disulfides, which contribute to low birefringence, in part because of reduced shrinkage effects and dynamic bond relaxation, especially when compared to conventional (photo)polymerizations such as (meth) acrylates. Finally, the high sulfur content directly incorporates polarizable sulfur atoms, which contribute to an increased refractive index and enable improved refractive index matching with the substrates to be adhered.[17] Because of these advan-

[a]Department of Chemical and Biological Engineering, University of Colorado Boulder, USA. E-mail: christopher.bowman@colorado.edu
[b]BioFrontiers Institute, University of Colorado Boulder, USA
[c]Polymer Chemistry Research group, Centre of Macromolecular Chemistry (CMaC) and Laboratory of Organic Synthesis, Department of Organic and Macromolecular Chemistry, Faculty of Sciences, Ghent University, Belgium
[d]Materials Science & Engineering Program, University of Colorado Boulder, USA

tages, dithiolanes have found widespread adoption for the creation of dynamic materials.[18–20]

Despite these advantages, the exploration of dithiolanes as adhesives has been relatively limited. For example, some dithiolane derivatives (*e.g.*, lipoic acid) had been used to create pressure sensitive,[21–23] structural,[24,25] and surgical adhesives; however, many of these reported adhesives are simple linear polymers driven by evaporative or thermal polymerizations.[26] More recent formulations have taken advantage of pendant dithiolanes functionalities to enable on-demand photocuring.[20,27,28] Since optical adhesives require transmittance above 95%,[29] both the dithiolane concentration and conversion must be managed to allow suitable transmittance, refractive index, and crosslinking density. Balancing effective crosslinking with effective optical performance is essential to realizing the successful development of a fully biobased adhesive system. Additionally, materials applied in optical elements have strict standards regarding yellowing, with photoinitiator fragments often being the source of post-polymerization colored products.[30] When coupled with suitable core structures (small molecules with limited crystallinity), no solvent is needed during application, resulting in resins capable of complete incorporation with no extractables at full conversion.

While many dithiolane adhesives have relied on coordination bonding,[25,26] supramolecular assembly,[31] or branching,[32] few have investigated the role of hydrogen bonding. In other materials, amide functionalities have primarily been used to increase hydrogen bonding in materials as a strategy to increase T_g and crystallinity.[33] However, urethane linkages remain the dominant strategy for increasing hydrogen bonding in materials.[34,35] While the use of urethanes in dithiolane adhesives has only recently been explored,[27,36] these studies involved the use of isocyanates to produce urethane bonds. Recently, isocyanate-free synthesis of urethane linkages has emerged as an alternative strategy for incorporating enhanced hydrogen bonding into adhesives without the need for phosgene, as is needed in the classical synthesis of isocyanates.[37] This strategy has previously been coupled with bisfunctional amines for the biobased synthesis of isocyanate-free polyurethanes.[38] Utilizing a cyclic carbonate, a β-hydroxyurethane can be produce through the reaction with an amine without the need for an isocyanate. For simplicity, this β-hydroxyurethane linkage is referred to as a urethane throughout. Taken together, using esters, urethanes, and amides as coupling chemistries results in a tunable library of hydrogen bonding in adhesives as a method to modulate material properties.

Recently, hydrogen bonding has been increasingly studied in adhesive systems both as an energy dissipation mechanism[39] and as a surface adhesion promoter.[40] These reversible interactions enhance surface contact through specific intermolecular attractions while also acting as sacrificial bonds that break and reform during deformation, increasing energy dissipation and therefore increasing toughness, especially when combined with other dynamic chemistries.[39] As a result, hydrogen bonding has been applied to traditional structural adhesives,[41] pressure sensitive adhesives,[42] surgical adhesives,[43] and optical adhesives.[44] Additionally, hydrogen bonding has seen increased utilization in natural systems that seek to replace petroleum-derived adhesives.[45] Combined with the photopolymerizability of dithiolanes, tunable hydrogen bonding offers a route to adhesive systems with enhanced bonding and tunable mechanical properties in biobased optical adhesives.

Herein, fully biobased 1,2-dithiolane-derived photocurable crosslinkers are synthesized by functionalizing Priamine and Pripol cores with lipoic acid *via* ester, amide, and urethane linkages, enabling controlled degrees of hydrogen bonding, all from biobased precursors. Because of the intrinsic ring-strain, these 1,2-dithiolane-based crosslinkers undergo initiator-free photolytic ring-opening polymerization upon UV irradiation over relatively short timescales. The resulting optical adhesives are tunable and exhibit low optical dispersion and high clarity. Their mechanical, adhesive, and optical properties were evaluated and correlated to the extent of hydrogen bonding present in the system. This strategy represents an advancement in the development of sustainable, non-petroleum-derived optical adhesives with excellent clarity and low dispersion. This work establishes a structure–property relationship between hydrogen bond strength and multiple material, adhesive, and optical properties in fully biobased dithiolane crosslinked optical adhesives as a means for showing their overall feasibility in these applications.

Results and discussion

To synthesize the optical adhesives, the biobased bisfunctional precursors Priamine 1074 and Pripol 2033 were functionalized with lipoic acid, either directly or *via* incorporation of a glycerol carbonate spacer to form urethane linkages without the need for isocyanates (Fig. 1a). Pripol 2033 was used to prepare ester-linked bisfunctional dithiolanes *via* Steglich esterification (Fig. S1), whereas Priamine 1074 was employed to synthesize both amide-linked (Fig. S2) and urethane-linked bisfunctional dithiolanes. For the synthesis of the urethane, the biobased glycerol carbonate was conjugated to lipoic acid with an ester to form lipoic acid glycerol carbonate (LA-GCC, Fig. S3), followed by ring-opening of the cyclic carbonate with Priamine, resulting in formation of the urethane (Fig. S4). The resulting series provides a library of precursors containing systematic variations in the hydrogen bonding strength, with ester-linked adhesives lacking hydrogen bonding, urethane linkages introducing moderate hydrogen bonding, and amides exhibiting the strongest hydrogen-bonding interactions (Fig. 1b).[46,47] In addition, a 50 : 50 mixture of ester- and amide-linked monomers that was photopolymerized into a polymer network (hereafter referred to as mixture) was also investigated as an intermediate hydrogen bonding case, further demonstrating the hydrogen bond strength modulation.

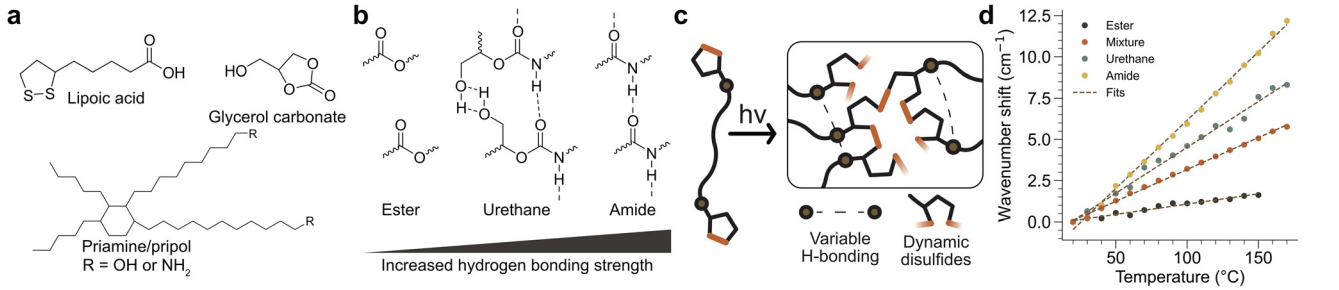

Fig. 1 Biobased dithiolane adhesives. (a) Biobased precursors used in the creation of dithiolane adhesives. (b) The hydrogen bond strength increases, moving from the ester to the urethane to the amide linker. (c) Schematic of dithiolane adhesive photocrosslinking, subsequent dynamic disulfide crosslinks, and variable hydrogen bond strength in the adhesive. (d) Centroid location of the C═O stretch during heating in FTIR.

Because of the intrinsic absorption of the dithiolane ring at relevant wavelengths (*i.e.*, 365 nm) (Fig. S5), the network precursors are capable of undergoing direct photolytic ring-opening polymerization (Fig. 1c). Films were prepared through direct photopolymerization, and the hydrogen bond strength was directly assessed *via* Fourier transform infrared (FTIR) spectroscopy. Specifically, FTIR of crosslinked samples was used to track the centroid of the C═O stretch over a wide temperature interval, ranging from 20 to 170 °C with +10 °C intervals (Fig. S6). The net displacement of this centroid over the course of the heating program was used as a proxy for hydrogen bond strength, and the slope of this displacement as a function of temperature was used as a quantitative measure of hydrogen bond strength throughout, as has been previously reported (Fig. 1d).[48] The trends observed here confirm the anticipated order of hydrogen bond strength in the materials: ester < mixture < urethane < amide.

To investigate curing behavior, isothermal photorheology was performed by applying a constant small-amplitude oscillatory shear (T = 25 °C, γ = 1%, ω = 1 rad s^{-1}) over a defined time period. For this characterization, the sample was first allowed to equilibrate in the darkness for 30 s after which polymerization was initiated by UV irradiation (50 mW cm^{-2} at 365 nm) while simultaneously monitoring and the evolution of the shear storage (G') and loss (G'') moduli (Fig. 2a). All formulations polymerized on relatively short timescales, reaching plateau moduli within 300 s. Taking this reaction rate into account, and to minimize effects of light attenuation, 50 μm adhesive films were produced by exposure to 50 mW cm^{-2} of 365 nm light for 2.5 min per side for all subsequent films. Notably, the urethane sample exhibited the slowest polymerization rate and achieved a final plateau modulus lower than the other resins. This behavior might potentially be attributed to the presence of free hydroxyls, resulting from the cyclic carbonate ring-opening. Free hydroxyl functionalities have previously been reported to affect dithiolane polymerization, leading to overall shorter kinetic chains despite similar conversion rates.[49,50] Therefore, it is postulated that the urethane sample has shorter dithiolane kinetic chains than the other three samples, leading to a lower crosslinking density and potentially explaining both the slower polymerization and lower storage modulus in the urethane sample.

The influence of variable hydrogen bond strength was further evaluated *via* dynamic mechanical analysis (DMA). In the glassy regime, the storage modulus was found to increase systematically with hydrogen bonding, with the ester sample having the lowest modulus and progressively higher values observed across the series (Fig. 2b). This trend was not observed in the rubbery regime, as the hydrogen bonds do not contribute to effective crosslinks in the rubbery modulus at this time scale. Rather, the rubbery storage modulus is virtually the same across the tested samples, except for the

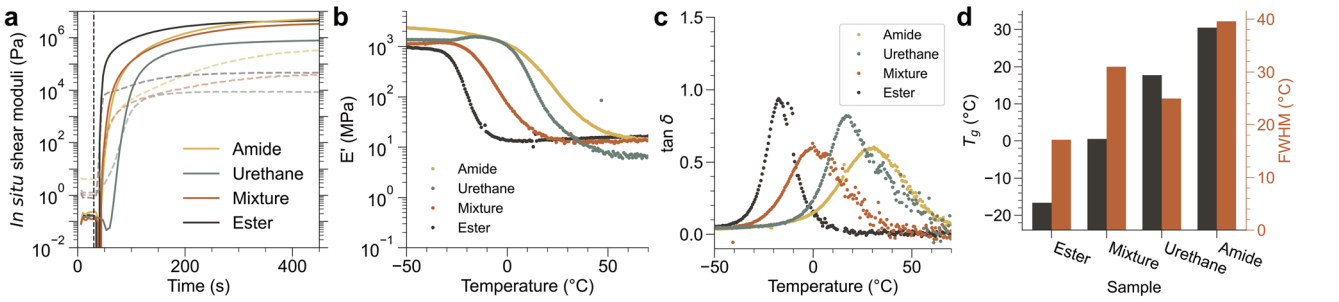

Fig. 2 Mechanical properties of dithiolane adhesives. (a) *In situ* photorheology of dithiolane adhesive crosslinking (50 mW cm^{-2}, 365 nm, 25 μm thick). (b) E' as a function of temperature in photocrosslinked films. (c) tan δ as a function of temperature in photocrosslinked films. (d) Glass transition temperature and FWHM as calculated from the tan δ in (c). T_g was additionally measured with dynamic scanning calorimetry in Fig. S7. All films polymerized 2.5 min per side, 50 mW cm^{-2} at 365 nm, 50 μm thick adhesive.

urethane, which had a decreased crosslink density. Furthermore, hydrogen bond strength was also found to have a strong effect on the glass transition (T_g) of the samples. As expected, increasing the strength of the hydrogen bonds leads to a systematic increase in the T_g of the samples (Fig. 2c).[51] In addition, the breadth of the glass transitions generally increases with additional hydrogen bonding (Fig. 2d). However, the urethane sample exhibited an unusually narrow T_g for its location in the hydrogen bonding series. This behavior may result from the same disruption of dithiolane polymerization (shorter kinetic chain lengths) that is speculated to contribute to the decreased rubbery modulus; shorter kinetic chains likely lead to a more homogenous network and therefore a narrower glass transition. These trends in T_g as measured by DMA are recapitulated in differential scanning calorimetry (DSC), again with the same anomaly in the breadth of the urethane T_g (Fig. S7).

As solvent resistance is an important characteristic of optical adhesives, the swelling ratio in mulitple solvents (toluene, acetone, methanol, and water) was tested for each sample (Fig. S8). Unsurprisingly, the swelling ratio trended with hydrogen bond strength, with the amide adhesive having the lowest swelling ratios, being as low as 1.2 in water (Fig. S8). In addition, limited extractables are key to adhesive performance. Samples tested *via* extraction in acetone demonstrated greater than 95% gel fraction (less than 5% extractable) across all formulations (Fig. S9). Additionally, flexibility is key for optical adhesives as they are often used to laminate thin films in flexbile electronics. These adhesives are highly flexible, as demonstrated through twisting a 50 μm thick amide sample between tweezers (Fig. S10). Lastly, while long term stability of materials used as adhesives is important for broad commercial adoption, an evaluation of long term aging is beyond the scope of this work. Generally, dithiolane-crosslinked materials exhibit good stability below temperatures of 120 °C, often well above the range of operating temperatures for optical materials outside of specialty applications.[52]

Next, the adhesive properties of the cured materials were evaluated by lap shear testing using both glass and poly(ethylene terephthalate) as substrates, with three replicate samples tested per condition (Fig. 3a). While peel is an important failure mode for optical adhesives, lap shear was chosen as an adhesion metric to correlate with hydrogen bond strength, given that these materials are photocured structural adhesives rather than pressure sensitive adhesives. Transparent substrates were chosen to enable photocuring of the adhesives and due to their relevance in optical applications. Notably, all measurements were taken without applying any adhesion promoters on the substrate surface. While this approach likely leads to a lower ultimate tensile strength, it enables a direct comparison of the effects of the hydrogen bond strength and their interactions with the substrate surface on adhesion. For glass substrates, no clear trend in either the lap shear strength or the strain at break (Fig. 3b and Fig. S10) was observed. Although intermediate-strength hydrogen bond systems (such as the mixture and urethane) exhibited the highest lap shear strength and strain at break, all samples had large errors associated with the measurements. This error is likely due to interfacial adhesive failures with the substrates, which are more stochastic than cohesive failures, especially in the absence of adhesion promoters.

In contrast, for plasma treated PET or PMMA substrates, both lap shear strength and strain at break generally increased with hydrogen bonding strength and had significantly lower variability (Fig. 3c, d and Fig. S11, S12). One potential explanation is the difference in the surface chemistry and roughness. Contact angle measurements with water reveal increased hydrophobicity in both the PMMA and the plasma treated PET as compared to glass (66° on PMMA *vs.* 59° on PET *vs.* 36° on glass, Fig. S14), indicating notable differences in surface chemistry and wettability. Compared to the relatively smooth glass microscope slides, the polymeric substrates may facilitate additional mechanical interlocking at the interface. Both factors contribute to PMMA and PET samples having more

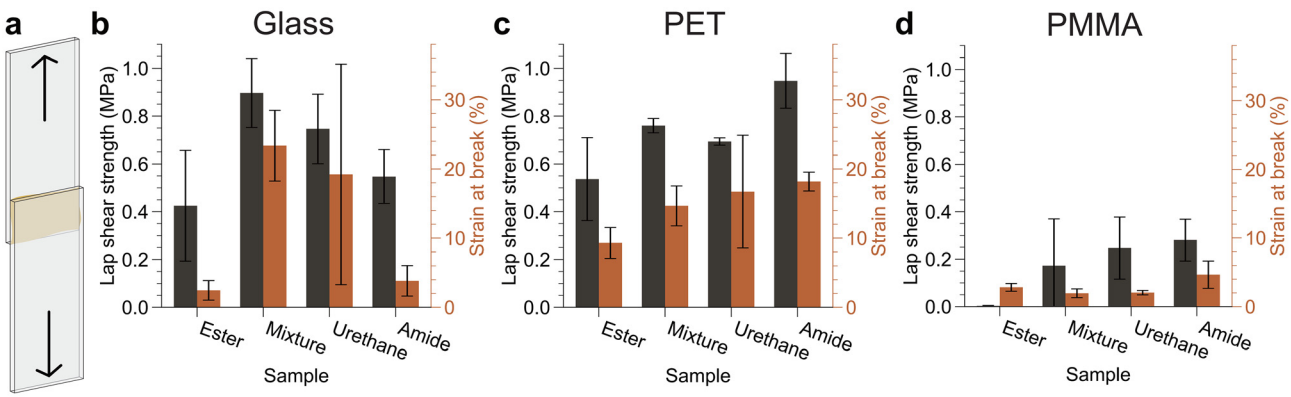

Fig. 3 Lap shear adhesive testing of dithiolane adhesives. (a) Schematic of lap shear setup, where two substrates are bonded together at an overlapping joint with adhesive and photocured. (b) Lap shear strength (left axis) and strain at break (right axis) for samples prepared with a glass substrate. (c) Lap shear strength (left axis) and strain at break (right axis) for samples prepared with a PET substrate. (d) Lap shear strength (left axis) and strain at break (right axis) for samples prepared with a PMMA substrate. All samples polymerized 2.5 min per side, 50 mW cm^{-2} at 365 nm, and 50 μm thick adhesive, with three replicates per condition. Error bars represent standard deviation.

cohesive failure modes, while the glass had more adhesive failure modes (Fig. S15). While these were the predominant modes observed through the lap shear stress–strain curves and sample examination, there is not conclusive evidence to determine that these failure modes are the only ones occurring for all cases.

As previously stated, optical adhesives must meet stringent performance criteria. For instance, high transmittance and low dispersion (high Abbe number) are critical for optically transparent adhesives.[1] All formulations had a high optical clarity, as demonstrated in a transmittance photograph of the amide sample between two glass substrates (Fig. 4a). UV-vis spectroscopy, performed on all samples between glass slides after curing, confirmed >98% transmittance across the visible portion of the spectrum for all samples (Fig. 4b), comparable to other optical materials based on sulfur chemistry.[53] Additionally, the adhesives exhibited minimal haze, as measured according to the ASTM D1003 standard: all samples measured below 0.3% haze, except for the mixture which had 0.7% haze (Fig. S16). Since the one sample that exhibited the higher haze is a mixture of two hydrogen bonding strengths, this increase in haze is potentially attributed to a small extent of micro-phase separation.

Refractive index (RI) modulation is another critical property for optical adhesives, as the adhesive must have a relatively close match in refractive index with the substrate to minimize optical aberrations. The RI was measured at 22 °C using a prism coupler refractometer and monochromatic light sources at three wavelengths (λ): 404.7 nm, 524.7 nm and 636.6 nm. Refractometry measures the angular position of total internal reflection. Utilizing PET as the substrate enhanced the substrate and film refractive index difference, minimizing any contributions of the substrate effect. The obtained RI were then fitted to the Cauchy equation (Fig. 4c) and used to interpolate the refractive index at the Fraunhofer D line (n_D, λ = 589.3 nm) for cross-comparison of all formulations. Notably, the refractive index was found to systematically increase with hydrogen bond strength (Fig. 4d). This difference is postulated to result from an increased density of the materials as expected from the Lorenz-Lorentz theorem, which correlates the density and polarizability of a material to its refractive index.[54–56] However, no clear trend was observed in the Abbe number (V_d), a measure of optical dispersion across wavelengths, which often decreases with increasing refractive index (Fig. S17). Regardless, V_d was comparatively high (representing low optical dispersion) for each of these materials.

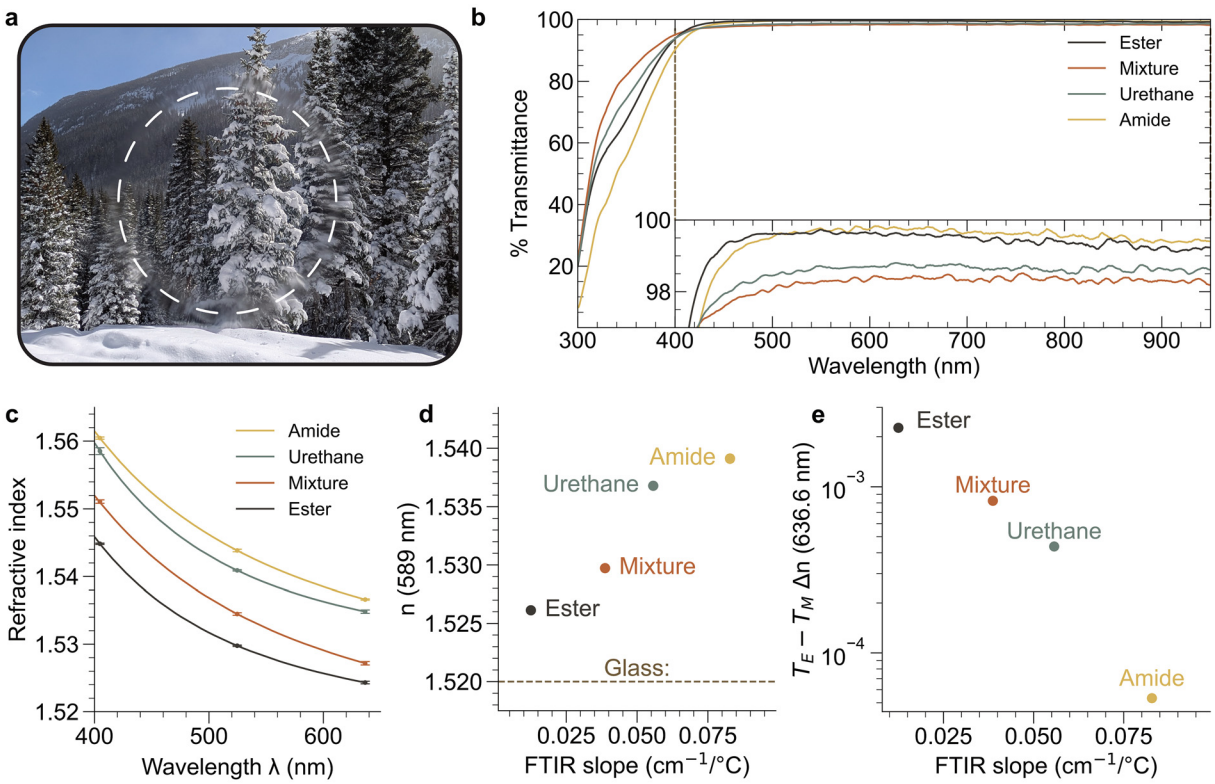

Fig. 4 Optical properties of dithiolane adhesives. (a) High transmittance image of a mixture sample between glass substrates. Dashed white line indicates adhesive boundary. (b) Transmittance through each formulation post curing between glass substrates. Inset shows zoomed region between 400 and 950 nm. (c) Refractive index as measured on samples polymerized on PET substrate. Cauchy fit curves of each sample, with the mean and standard deviation of each measured wavelength highlighted (T_E polarization). (d) Refractive index trends with increasing hydrogen bonding as quantified by the slope of the centroid of the C=O stretch as a function of temperature in FTIR (T_E polarization). (e) Birefringence trends with hydrogen bonding (measured at 636.6 nm). All samples polymerized 2.5 min per side, 50 mW cm^{-2} at 365 nm, 50 μm thick adhesive.

Finally, birefringence was evaluated. This optical phenomenon originates from anisotropic effects in the molecular polarizability throughout the material and was quantified by taking the difference in refractive index for light polarized in two orthogonal directions. As many optical applications rely on varied polarizations, minimizing birefringence is of high priority, especially in comparison to commercial urethane-acrylate adhesives where anisotropic shrinkage often leads to stress-laden polymer films with increased birefringence.[57] To quantify this effect, the RI was quantified in both transverse electric (T_E) and transverse magnetic (T_M) polarization modes, with the difference between these values being the birefringence. At the measurement wavelength of 636.6 nm, increased hydrogen bonding strength results in lower birefringence (Fig. 4e). We speculate that increased hydrogen bond strength increases dynamic exchange, enabling further rearrangement after polymerization. Notably, these are all low birefringent materials, with the highest birefringence of 0.002 and the lowest at 0.00005 (below the error of the instrument) compared to many common plastics, such as polycarbonate (0.015), polystyrene (0.019), and even performance acrylates (0.002).[58] This property is likely due to the ring-opening polymerization of the dithiolanes, which minimizes shrinkage stress during the polymerization, as well as the delayed gelation and disulfide exchange from the polymerization.

Conclusion

In this work, fully biobased dithiolane adhesives with ester, urethane, and amide linkers, were synthesized, creating a library of adhesives with varied hydrogen bond strength. These materials are capable of photopolymerization without the need for exogenous initiator. Hydrogen bond strength was found to have a direct impact on a variety of material properties, including T_g, lap shear strength and strain at break on PET and PMMA substrates, RI, and birefringence. Furthermore, the high optical clarity and tunable refractive indices of these materials makes them well suited to optical adhesive applications. There is a clear structure–property relationship between the hydrogen bond strength and multiple material, adhesive and optical properties, establishing tunability of properties through hydrogen bond strength in these dithiolane-crosslinked, fully biobased optical adhesives.

Conflicts of interest

There are no conflicts of interest to declare.

Data availability

All data needed to evaluate the conclusions in the paper are present in the paper and/or the supplementary information (SI). Supplementary information is available. See DOI: https://doi.org/10.1039/d6lp00120c.

Raw data are available from the authors upon reasonable request.

Acknowledgements

The authors gratefully acknowledge funding from the Industry University Cooperative Research Center for Fundamentals and Applications of Photopolymerizations (C. N. B. and B. R. N.), and the National Heart, Lung, and Blood Institute (NHLBI, Grant number: R01 HL171197, K. S. A.). V. S. and F. D. P. would like to thank the Research Foundation Flanders (FWO) (Application 1S34725N and V410425N) for financial support. FEDP acknowledges BOF-UGent for GOA funding (BOF21/GOA/007). The authors would like to thank B. E. Kirkpatrick and J. Debuyck for their fruitful discussions, and S. A. Klug for experimental assistance.

References

1 Y. Du, Y. Li, C. Li, R. Xu, L. Meng and Y. Bai, *ACS Appl. Mater. Interfaces*, 2025, **17**, 5578–5594.
2 W. Ming, Z. Xie, Z. Jiang, Y. Chen, G. Zhang, Y. Xu and W. He, *J. Soc. Inf. Disp.*, 2022, **30**, 851–876.
3 G. Wang, Z. Zhou, M. Chen, J. Wang and Y. Yu, *ACS Appl. Polym. Mater.*, 2023, **5**, 2051–2061.
4 Y. Liu, M. L. Wu, Y. D. Li, L. Y. Li and J. B. Zeng, *ACS Sustainable Chem. Eng.*, 2023, **11**, 17190–17198.
5 L. Pezzana, G. Melilli, P. Delliere, D. Moraru, N. Guigo, N. Sbirrazzuoli and M. Sangermano, *Prog. Org. Coat.*, 2022, **173**, 107949.
6 J. A. Mclaughlin, E. Kinaci and G. R. Palmese, *ACS Appl. Polym. Mater.*, 2024, **6**, 11733–11742.
7 L. Pezzana and M. Sangermano, *Prog. Org. Coat.*, 2021, **157**, 106295.
8 F. Van Lijsebetten, T. Maiheu, J. M. Winne and F. E. Du Prez, *Adv. Mater.*, 2023, **35**, e2300802.
9 S. Liang, H. Zhao, X. Li, Y. Feng and J. Zhao, *ACS Appl. Polym. Mater.*, 2024, **6**, 9615–9626.
10 P. Ranganathan, C.-W. Chen, M.-C. Tasi, S.-P. Rwei and Y.-H. Lee, *Ind. Eng. Chem. Res.*, 2021, **60**, 12139–12154.
11 C. R. Frihart, *Polymers*, 2023, **15**, 3345.
12 R. F. R. Freitas, C. Klein, M. P. Pereira, R. B. Duczinski, S. Einloft, M. Seferin and R. Ligabue, *J. Adhes. Sci. Technol.*, 2015, **29**, 1860–1872.
13 J. Liu, K. Wang, Y. Xie, F. Gao, Q. Zeng, Y. Yuan, R. Liu and X. Liu, *J. Coat. Technol. Res.*, 2017, **14**, 1325–1334.
14 L. J. Reed, B. G. Debusk, I. C. Gunsalus and G. H. F. Schnakenberg, *J. Am. Chem. Soc.*, 1951, **73**, 5920.
15 J. A. Barltrop, P. M. Hayes and M. Calvin, *J. Am. Chem. Soc.*, 1954, **76**, 4348–4367.
16 R. B. Whitney and M. Calvin, *J. Chem. Phys.*, 1955, **23**, 1750–1756.
17 S. P. Keyser, M. Trujillo-Lemon, A. N. Sias, B. D. Fairbanks, R. R. McLeod and C. N. Bowman, *ACS Appl. Mater. Interfaces*, 2024, **16**, 45577–45588.

18 C. Choi, J. L. Self, Y. Okayama, A. E. Levi, M. Gerst, J. C. Speros, C. J. Hawker, J. Read de Alaniz and C. M. Bates, *J. Am. Chem. Soc.*, 2021, **143**, 9866–9871.
19 Q. Zhang, Y. X. Deng, H. X. Luo, C. Y. Shi, G. M. Geise, B. L. Feringa, H. Tian and D. H. Qu, *J. Am. Chem. Soc.*, 2019, **141**, 12804–12814.
20 B. Sieredzinska, Q. Zhang, K. Berg, J. Flapper and B. L. Feringa, *Chem. Commun.*, 2021, **57**, 9838–9841.
21 K. R. Albanese, Y. Okayama, P. T. Morris, M. Gerst, R. Gupta, J. C. Speros, C. J. Hawker, C. Choi, J. R. de Alaniz and C. M. Bates, *ACS Macro Lett.*, 2023, **12**, 787–793.
22 K. V. Dikshit, A. M. Visal, F. Janssen, A. Larsen and C. J. Bruns, *ACS Appl. Mater. Interfaces*, 2023, **15**, 17256–17267.
23 S. Luo, N. Wang, Y. Pan, B. Zheng, F. Li and S. Dong, *Small*, 2024, **20**, e2310839.
24 Y. Deng, Q. Zhang, C. Shi, R. Toyoda, D. H. Qu, H. Tian and B. L. Feringa, *Sci. Adv.*, 2022, **8**, eabk3286.
25 Q. Zhang, C. Y. Shi, D. H. Qu, Y. T. Long, B. L. Feringa and H. Tian, *Sci. Adv.*, 2018, **4**, eaat8192.
26 S. Pal, J. Shin, K. DeFrates, M. Arslan, K. Dale, H. Chen, D. Ramirez and P. B. Messersmith, *Science*, 2024, **385**, 877–883.
27 Z. Q. Liu, C. Z. Ju, P. L. Li, Z. C. Yan and Z. Zhang, *J. Appl. Polym. Sci.*, 2025, **142**, e56520.
28 S. Maes, V. Scholiers and F. E. Du Prez, *Macromol. Chem. Phys.*, 2022, **224**, 2100445.
29 S.-W. Lee, J.-W. Park, C.-H. Park, Y.-E. Kwon, H.-J. Kim, E.-A. Kim, H.-S. Woo, S. Schwartz, M. Rafailovich and J. Sokolov, *Int. J. Adhes. Adhes.*, 2013, **44**, 200–208.
30 J. Segurola, N. S. Allen, M. Edge, A. McMahon and S. Wilson, *Polym. Degrad. Stab.*, 1999, **64**, 39–48.
31 H. Y. Lin, L. Li, Q. Zhang, D. H. Qu and F. Tong, *Chemistry*, 2025, **31**, e202500900.
32 S. Pal, E. E. Salzman, D. Ramirez, H. Chen, C. A. Perez, K. Dale, S. K. Ghosh, L. Lin and P. B. Messersmith, *J. Am. Chem. Soc.*, 2025, **147**, 13377–13384.
33 C. J. Reese, G. M. Musgrave, P. Cardon, H. Ji, M. Shusteff and C. Wang, *ACS Macro Lett.*, 2025, **14**, 1189–1194.
34 D. K. Chattopadhyay and K. V. S. N. Raju, *Prog. Polym. Sci.*, 2007, **32**, 352–418.
35 V. Scholiers, B. Hendriks, S. Maes, T. Debsharma, J. M. Winne and F. E. Du Prez, *Macromolecules*, 2023, **56**, 9559–9569.
36 Y. J. Zhou, N. N. Xia, J. L. Zhang, T. X. Li, J. M. Wang and Q. Wu, *ACS Sustainable Chem. Eng.*, 2025, **13**, 6412–6422.
37 L. Maisonneuve, O. Lamarzelle, E. Rix, E. Grau and H. Cramail, *Chem. Rev.*, 2015, **115**, 12407–12439.
38 K. Błażek, P. Kasprzyk and J. Datta, *Polymer*, 2020, **205**, 122768.
39 S. Chen, K. Zhang, Z. Li, Y. Wu, B. Zhu and J. Zhu, *Supramol. Mater.*, 2023, **2**, 100032.
40 K. Viswanathan, H. Ozhalici, C. L. Elkins, C. Heisey, T. C. Ward and T. E. Long, *Langmuir*, 2006, **22**, 1099–1105.
41 W. Xiang and J. Xia, *ACS Omega*, 2024, **9**, 13644–13654.
42 M. M. Feldstein, E. E. Dormidontova and A. R. Khokhlov, *Prog. Polym. Sci.*, 2015, **42**, 79–153.
43 Q. Zhang, Z.-Y. Xu and W.-G. Liu, *Chin. J. Polym. Sci.*, 2024, **42**, 1619–1641.
44 C. Lin, B. Qin and J. Xia, *ACS Appl. Polym. Mater.*, 2025, **7**, 10686–10700.
45 S. Wu, C. Cai, F. Li, Z. Tan and S. Dong, *CCS Chem.*, 2021, **3**, 1690–1700.
46 J.-Y. Le Questel, C. Laurence, A. Lachkar, M. Helbert and M. Berthelot, *J. Chem. Soc., Perkin Trans. 2*, 1992, **12**, 2091–2094.
47 C. B. Berlin, E. Sharma and M. C. Kozlowski, *J. Org. Chem.*, 2024, **89**, 4684–4690.
48 M. T. Lemon, M. S. Jones and J. W. Stansbury, *J. Biomed. Mater. Res., Part A*, 2007, **83**, 734–746.
49 P. R. Brown and J. O. Edwards, *J. Org. Chem.*, 1969, **34**, 3131–3135.
50 P. R. Brown and J. O. Edwards, *J. Chromatogr.*, 1969, **43**, 515–518.
51 T. K. Kwei, *J. Polym. Sci., Polym. Lett. Ed.*, 1984, **22**, 307–313.
52 Q. Zhang, B. L. Feringa, D. H. Qu and H. Tian, *Acc. Chem. Res.*, 2026, **59**, 151–164.
53 S. S. Chen, V. Scholiers, H. Chen, X. W. An, J. J. Li, J. Zhu, F. E. Du Prez and X. Q. Pan, *Chin. J. Polym. Sci.*, 2025, **43**, 2022–2029.
54 S. Watanabe, T. Takayama and K. Oyaizu, *ACS Polym. Au*, 2022, **2**, 458–466.
55 B. Yuan, L. Tian, J. Bai, Y. Zhang, Y. Peng, J. Cui, Z. Fan, M. Guo, Y. Li and B. Cheng, *Polymer*, 2026, **348**, 129735.
56 B. F. Hanley, *Mater. Today Commun.*, 2020, **25**, 101644.
57 Y. Jeon, J. Choi, D. Seo, S. H. Jung and J. Lim, *Polym. Chem.*, 2023, **14**, 1117–1123.
58 Y. Tojo, Y. Arakwa, J. Watanabe and G.-i. Konishi, *Polym. Chem.*, 2013, **4**, 3807–3812.